

SARS-CoV-2 mRNA vaccines induce robust plasmablast and germinal centre responses in humans

Jackson S. Turner^{1*}, Jane A. O'Halloran^{2*}, Elizaveta Kalaidina³, Wooseob Kim¹, Aaron J. Schmitz¹, Tingting Lei¹, Mahima Thapa¹, Rita E. Chen^{1,4}, James Brett Case⁴, Fatima Amanat^{5,6}, Adriana M. Rausedo², Alem Haile⁷, Xuping Xie⁸, Michael K. Klebert⁷, Teresa Suessen⁹, William D. Middleton⁹, Pei-Yong Shi⁸, Florian Krammer⁵, Sharlene A. Teefey⁹, Michael S. Diamond^{4,10}, Rachel M. Presti^{2#}, and Ali H. Ellebedy^{1,10#}

¹Department of Pathology and Immunology, Washington University School of Medicine, St. Louis, MO, USA; ²Division of Infectious Diseases, Department of Internal Medicine, Washington University School of Medicine, St. Louis, MO, USA; ³Division of Allergy and Immunology, Department of Internal Medicine, Washington University School of Medicine, St. Louis, MO, USA; ⁴Department of Medicine, Washington University School of Medicine, St. Louis, MO, USA; ⁵Department of Microbiology, Icahn School of Medicine at Mount Sinai, New York, NY, USA; ⁶Graduate School of Biomedical Sciences, Icahn School of Medicine at Mount Sinai, New York, NY, USA; ⁷Clinical Trials Unit, Washington University School of Medicine, St. Louis, MO, USA; ⁸University of Texas Medical Branch, Galveston, TX, USA; ⁹Mallinckrodt Institute of Radiology, Washington University School of Medicine, St. Louis, MO, USA; ¹⁰The Andrew M. and Jane M. Bursky Center for Human Immunology & Immunotherapy Programs

*These authors contributed equally to this work

#Corresponding authors: Ali H. Ellebedy, Ph.D., ellebedy@wustl.edu, and Rachel M. Presti, M.D., Ph.D., prestir@wustl.edu

ABSTRACT

Severe Acute Respiratory Syndrome Coronavirus 2 (SARS-CoV-2) messenger RNA (mRNA)-based vaccines are ~95% effective in preventing coronavirus disease 2019¹⁻⁵. However, the dynamics of antibody secreting plasmablasts (PBs) and germinal centre (GC) B cells induced by these vaccines in SARS-CoV-2 naïve and antigen-experienced humans remains unclear. Here we examined peripheral blood and/or lymph node (LN) antigen-specific B cell responses in individuals who received two doses of BNT162b2, an mRNA-based vaccine encoding the full-length SARS-CoV-2 spike (S) gene¹. Circulating IgG- and IgA-secreting PBs targeting the S protein peaked one week after the second immunization then declined and were undetectable three weeks later. PB responses coincided with maximal levels of serum anti-S binding and neutralizing antibodies to a historical strain as well as emerging variants, especially in individuals previously infected with SARS-CoV-2, who produced the most robust serological responses. Fine needle aspirates of draining axillary LNs identified GC B cells that bind S protein in all participants sampled after primary immunization. GC responses increased after boosting and were detectable in two distinct LNs in several participants. Remarkably, high frequencies of S-binding GC B cells and PBs were maintained in draining LNs for up to seven weeks after first immunization, with a substantial fraction of the PB pool class-switched to IgA. GC B cell-derived monoclonal antibodies predominantly targeted the RBD, with fewer clones binding to the N-terminal domain or shared epitopes within the S proteins of human betacoronaviruses OC43 and HKU1. Our studies demonstrate that SARS-CoV-2 mRNA-based vaccination of humans induces a robust and persistent GC B cell response that engages pre-existing as well as new B cell clones, which enables generation of high-affinity, broad, and durable humoral immunity.

MAIN TEXT

The concept of using mRNAs as vaccines was first introduced over 30 years ago^{6,7}. Key refinements that improved the biological stability and translation capacity of exogenous mRNA enabled development of these molecules as vaccines^{8,9}. The emergence of SARS-CoV-2 in December, 2019 and the ensuing pandemic has unveiled the potential of this platform^{9–11}. In the United States, more than 80 million people have received one of the two SARS-CoV-2 mRNA-based vaccines that were granted emergency use authorization by the FDA in December, 2020. Both vaccines demonstrated remarkable immunogenicity in phase 1/2 studies and effectiveness in phase 3 studies^{1–4,12–14}. Whether these vaccines induce germinal center (GC) reactions that are critical for high-affinity and durable antibody responses has not been examined in humans. To address this question, we conducted an observational study of 32 healthy adults (7 with history of prior SARS-CoV-2 infection) who received the Pfizer-BioNTech SARS-CoV-2 mRNA vaccine (BNT162b2) (**Extended Data Table 1**). The two vaccine doses were injected in the deltoid muscle three weeks apart. Blood samples were collected at baseline and at weeks 3 (pre-boost), 4, 5, and 7 after the first immunization (**Fig. 1a**). Fine needle aspirates (FNAs) of the draining axillary lymph nodes were collected from 12 participants (none with history of SARS-CoV-2 infection) at weeks 3 (pre-boost), 4, 5, and 7 after the first immunization (**Fig. 1a**).

Antibody-secreting plasmablasts (PBs) that bound SARS-CoV-2 S protein were measured in blood using an enzyme-linked immune absorbent spot (ELISpot) assay. SARS-CoV-2-S-specific IgG- and IgA-secreting PBs were detected in blood three weeks after primary immunization in 19 of 25 participants with no history of SARS-CoV-2 infection but 0 of 7 participants previously infected with SARS-CoV-2. PBs peaked in blood during the first week after boosting (week 4) in all participants, with frequencies varying widely from 3 to 4,100 S-binding PBs per 10⁶ PBMC (**Fig. 1b, c**). Plasma IgG antibody titers against S measured by ELISA increased in all participants over time, reaching peak geometric mean half-maximal binding dilutions of 5,239 and 14,924 among participants without and with history of SARS-CoV-2

infection, respectively, and then declining slightly by seven weeks after immunization. IgG titers against the receptor binding domain (RBD) of S showed similar kinetics, reaching peak geometric mean half-maximal binding dilutions of 4,511 and 8,034 among participants without and with history of SARS-CoV-2 infection, respectively before declining (**Fig. 1d**). The functional quality of serum antibody titers was measured using high-throughput focus reduction neutralization tests (FRNTs)¹⁵ on Vero-TMPRSS2 cells against three authentic infectious SARS-CoV-2 strains with sequence variations in the S gene^{16,17}: (a) a Washington strain (2019n-CoV/USA) with a prevailing D614G substitution (WA1/2020 D614G); (b) a B.1.1.7 isolate with signature changes in the spike gene¹⁸, including the 69–70 and 144–145 deletions and N501Y, A570D, D614G and P681H substitutions; and (c) a chimeric SARS-CoV-2 with a B.1.351 spike gene in the Washington strain background (Wash SA-B.1.351) that contained the following changes: D80A, 242-244 deletion, R246I, K417N, E484K, N501Y, D614G and A701V. Serum neutralizing titers increased markedly in participants without history of SARS-CoV-2 infection following boosting, with geometric mean neutralization titers (GMTs) against D614G of 58.1 three weeks and 571.5 five or seven weeks after primary immunization. Neutralizing titers against B.1.1.7 and B.1.351 variants were lower, with GMTs of 48.9 and 373.2 against B.1.1.7 and 35.6 and 136.7 against B.1.351 after primary and secondary immunization, respectively. In participants with a history of prior SARS-CoV-2 infection, neutralizing titers against all three viruses were detected at baseline (GMTs of 241.8, 201.8, and 136.7 against D614G, B.1.1.7, and B.1.351 respectively). In these participants, neutralizing titers increased more rapidly after immunization, with GMTs of 4,544.1, 3,584.1, and 1,897.1 against D614G, B.1.1.7, and B.1.351, respectively after primary immunization, and 9,381.2, 9,351.4, and 2,748.6 against D614G, B.1.1.7, and B.1.351 respectively after secondary immunization. These GMTs were 78-, 73-, and 53-fold higher after primary immunization and 16-, 25-, and 20-fold higher after boosting against D614G, B.1.1.7, and B.1.351, respectively than participants without history of SARS-CoV-2 infection. (**Fig. 1e**).

The BNT162b2 vaccine is injected into the deltoid muscle, which drains primarily to the lateral axillary lymph nodes. Ultrasound was used to identify and guide FNA of accessible axillary nodes on the side of immunization approximately 3 weeks after primary immunization. In 5 of the 12 participants, a second draining LN was identified and sampled following secondary immunization (**Fig. 2a**). GC B cells, defined as CD19⁺ CD3⁻ IgD^{lo} Bcl6⁺ CD38^{int} lymphocytes, were detected in all LNs (**Fig. 2b, c, Extended Data Fig. 1a**). FNA samples were co-stained with two fluorescently labeled S probes to detect S-binding GC B cells. A control tonsillectomy sample with a high frequency of GC B cells collected prior to the SARS-CoV-2 pandemic from an unrelated donor was stained as a negative control. S-binding GC B cells were detected in FNAs from all 12 participants following primary immunization. Kinetics of the GC response varied among participants, but S-binding GC B cell frequencies increased at least transiently in all participants after boosting and persisted at high frequency in most individuals for at least 7 weeks (**Fig. 2d, e, Extended Data Fig. 1b**).

To evaluate the domains targeted by the S protein-specific GC response after vaccination, we generated recombinant monoclonal antibodies (mAbs) from single-cell sorted S-binding GC B cells (defined by the surface marker phenotype CD19⁺ CD3⁻ IgD^{lo} CD20^{hi} CD38^{int} CD71⁺ CXCR5⁺ lymphocytes) from three of the participants one week after boosting (**Extended Data Fig. 1a**). Nine, three, and eleven S-binding, clonally distinct mAbs were generated from participants 07, 20, and 22, respectively. Clonal relatives of 1, 3, and 4 of the mAbs were identified among 21, 46, and 55 heavy chain Ig sequences from participants 07, 20, and 22, respectively, indicating clonal expansion of B cells encoding these mAbs (**Extended Data Table 3**). Of the 23 mAbs, 14 bound RBD, 3 recognized the N-terminal domain, and 2 were cross-reactive with spike proteins from seasonal betacoronavirus OC43; one of these mAbs also bound spike from seasonal betacoronavirus HKU1 (**Fig. 2f**).

In addition to GC B cells, robust PB responses were detected in the draining LNs of all 12 participants sampled. S-binding PBs, defined as CD19⁺ CD3⁻ IgD^{lo} CD20^{lo} CD38⁺ CD71⁺ Blimp1⁺

lymphocytes, were detected in all LNs sampled and increased in frequency after boosting (**Fig. 3a, b**). The detected lymph node PBs were unlikely a contaminant of blood because CD14⁺ monocyte/granulocyte frequencies were below 1% in all FNA samples, well below the 10% threshold we previously established¹⁹. Moreover, S-binding PBs were detected in FNA samples 5 and 7 weeks after primary immunization, when they had become undetectable in blood from all participants in the cohort. The vast majority of S-binding LN PBs were isotype-switched 5 weeks after primary immunization, and IgA-switched cells accounted for 25% or more of the PBs in 6 of 12 participants (**Fig. 3c, d**).

This study evaluated whether SARS-CoV-2 mRNA-based vaccines induce antigen-specific GC cell responses in humans. The vaccine induced a strong IgG-dominated PB response in blood that peaked one week after the booster immunization. In the draining lymph nodes, we detected robust SARS-CoV-2 S-binding GC and PB responses in aspirates from 12 of 12 participants. These responses were detectable after the first immunization and increased after the second. Notably, S-binding GC B cells and PBs persisted for up to seven weeks after the first immunization. These results with mRNA vaccines are superior to those seen after seasonal influenza virus vaccination in humans¹⁹, where hemagglutinin-binding GC B cells were detected in only three of eight participants. More robust GC responses are consistent with antigen dissemination to multiple LNs and the self-adjuncting characteristics of the mRNA/lipid nanoparticle vaccine platform compared to nonadjuvanted protein subunit vaccines used for seasonal influenza virus vaccination^{7,20,21}. Our data in humans corroborate reports demonstrating the induction of potent GC responses by SARS-CoV-2 mRNA-based vaccines in mice^{22,23}.

Apart from the PB response in blood, the S-specific PB pool that persists in the draining lymph nodes contained a substantial fraction of IgA⁺ cells. This observation is intriguing because it occurred after intramuscular rather than mucosal vaccination²⁴. Although none of the lymph node aspirates we collected came from subjects with a prior history of SARS-CoV-2 infection, it remains possible that the IgA⁺ PBs originated from pre-existing IgA⁺ memory B cells induced by previous

upper respiratory infection with a seasonal human coronavirus. The precise contribution of IgA⁺ PBs to the total antigen-specific serum IgA response and efficacy of mRNA vaccines in humans requires further study and analysis. It also remains to be elucidated how related the PB clones detected in the draining LNs are to those within the GC and to those that become long-lived plasma cells in the bone marrow.

Although comparing the dynamics of B cell responses to SARS-CoV-2 vaccination in individuals with and without history of confirmed SARS-CoV-2 infection was not one of the original study objectives, differences in the kinetics of circulating S-specific plasmablast and serum antibody responses were apparent. S-specific IgG-secreting plasmablasts were detectable at the 3-week time point after the first immunization only in the group with no prior history of SARS-CoV-2 infection. This is consistent with the expected extended kinetics of a primary PB response. PBs responding to the first immunization in the individuals primed by SARS-CoV-2 infection most likely disappear from blood by two weeks after vaccination, consistent with the dynamics of recall responses observed after seasonal influenza virus vaccination^{19,25,26}. This finding is consistent with the sharp increase of S-binding and neutralizing antibodies in serum after primary immunization in the virus-experienced group²⁷. Notably, serum neutralizing antibody titers against the predominant circulating SARS-CoV-2 strain and recent variants were substantially higher in the previously infected group. This result was likely driven by the engagement of affinity matured S-specific memory B cell clones generated before vaccination²⁸. These findings indicate that individuals infected early during the pandemic then vaccinated may have a higher likelihood of protection against infection with the more recent isolates, including those containing the E484K mutation.

A preliminary finding from our study is the dominance of RBD-targeting clones among responding GC B cells. For the most part, these clones harbored few (<3) non-synonymous nucleotide substitutions in the immunoglobulin heavy chain variable genes, indicating that they originated from recently engaged naïve B cells. This contrasts with the two cross-reactive GC B

cell clones that recognized conserved epitopes within the spike proteins of betacoronaviruses. The cross-reactive clones accumulated 12 or more non-synonymous nucleotide substitutions, indicating a memory B cell origin. These data are consistent with previous findings from seasonal influenza virus vaccination in humans showing that the GC reaction can engage pre-existing memory B cells directed against conserved epitopes as well as naïve clones targeting novel epitopes¹⁹. These observations are important in the context of the emergence of multiple SARS-CoV-2 variants that can partially evade pre-existing serum neutralizing antibody responses¹⁷. This concern has prompted the design of SARS-CoV-2 variant-based vaccine candidates. Our data suggest these variant vaccines might engage pre-existing as well as new B cell clones specific to the variant S proteins even when given to people previously immunized with one of the original SARS-CoV-2 vaccine formulations.

Limitations of the study. Our study provides direct evidence for the induction of antigen specific GC B cell responses after mRNA vaccination in humans. Nonetheless, we acknowledge several limitations. We analyzed B cell responses over a relatively brief period (seven weeks) after the first SARS-CoV-2 mRNA immunization. While this allowed for interrogation of the acute vaccine-induced immune response, the durability of such responses remains unclear. A majority of the serum antibody response we analyzed likely originated from short lived PBs. Indeed, S-binding antibody titers declined beginning five weeks after primary immunization. Longer-term analyses are required to determine the decay rates of antibody responses induced by the mRNA vaccine platforms. As part of such studies, it will also be important to examine whether mRNA vaccination induces an S-specific long-lived plasma cell compartment in the bone marrow. The persistence of S-binding GC B cells and PBs in draining lymph nodes is a positive indicator for induction of long-lived plasma cell responses²⁹. Another limitation is the relatively small number of GC B cell-derived mAbs generated from only three individuals. A comprehensive set of mAbs derived from PBs and GC B cells of more individuals will help to define the breadth of the antibody response elicited by this vaccine. None of the 12 participants in our study who underwent biopsy

of draining lymph nodes had a history of prior SARS-CoV-2 infection. Thus, further comparison of vaccine-induced GC responses from naïve and previously infected individuals will be informative. Finally, the work presented here focuses on the B cell component of the GC response. A robust T follicular helper response sustains the GC reaction³⁰. As such, studies are planned to interrogate the magnitude, specificity, and durability of the T follicular helper response after SARS-CoV-2 mRNA vaccination in humans.

Overall, our data demonstrate a remarkable capacity of SARS-CoV-2 mRNA-based vaccines to induce robust GC reactions. Importantly, the GC response was maintained for an extended period following vaccination. The induced GC reaction recruited pre-existing cross-reactive memory B cell clones as well as newly engaged ones that target unique epitopes within SARS-CoV-2 S protein. Elicitation of high affinity and durable protective antibody responses is a hallmark of a successful humoral immune response to vaccination. By inducing robust GC reactions, SARS-CoV-2 mRNA-based vaccines are on track for achieving this outcome.

References

1. Mulligan, M. J. *et al.* Phase I/II study of COVID-19 RNA vaccine BNT162b1 in adults. *Nature* **586**, 589–593 (2020).
2. Jackson, L. A. *et al.* An mRNA Vaccine against SARS-CoV-2 — Preliminary Report. *N. Engl. J. Med.* **383**, 1920–1931 (2020).
3. Sahin, U. *et al.* COVID-19 vaccine BNT162b1 elicits human antibody and TH1 T cell responses. *Nature* **586**, 594–599 (2020).
4. Polack, F. P. *et al.* Safety and Efficacy of the BNT162b2 mRNA Covid-19 Vaccine. *N. Engl. J. Med.* **383**, 2603–2615 (2020).
5. Baden, L. R. *et al.* Efficacy and Safety of the mRNA-1273 SARS-CoV-2 Vaccine. *N. Engl. J. Med.* **384**, 403–416 (2021).

- 227 6. Zhou, X. *et al.* Self-replicating Semliki Forest virus RNA as recombinant vaccine. *Vaccine* **12**, 1510–
228 1514 (1994).
- 229 7. Cagigi, A. & Loré, K. Immune Responses Induced by mRNA Vaccination in Mice, Monkeys and
230 Humans. *Vaccines* **9**, 61 (2021).
- 231 8. Karikó, K. *et al.* Incorporation of Pseudouridine Into mRNA Yields Superior Nonimmunogenic Vector
232 With Increased Translational Capacity and Biological Stability. *Mol. Ther.* **16**, 1833–1840 (2008).
- 233 9. Schlake, T., Thess, A., Fotin-Mleczek, M. & Kallen, K.-J. Developing mRNA-vaccine technologies. *RNA*
234 *Biol.* **9**, 1319–1330 (2012).
- 235 10. Graham, B. S., Mascola, J. R. & Fauci, A. S. Novel Vaccine Technologies: Essential Components of an
236 Adequate Response to Emerging Viral Diseases. *JAMA* **319**, 1431 (2018).
- 237 11. Bettini, E. & Locci, M. SARS-CoV-2 mRNA Vaccines: Immunological Mechanism and Beyond. *Vaccines*
238 **9**, 147 (2021).
- 239 12. Amit, S., Regev-Yochay, G., Afek, A., Kreiss, Y. & Leshem, E. Early rate reductions of SARS-CoV-2
240 infection and COVID-19 in BNT162b2 vaccine recipients. *The Lancet* **397**, 875–877 (2021).
- 241 13. Dagan, N. *et al.* BNT162b2 mRNA Covid-19 Vaccine in a Nationwide Mass Vaccination Setting. *N.*
242 *Engl. J. Med.* NEJMoa2101765 (2021) doi:10.1056/NEJMoa2101765.
- 243 14. Vasileiou, E. *et al.* Effectiveness of First Dose of COVID-19 Vaccines Against Hospital Admissions in
244 Scotland: National Prospective Cohort Study of 5.4 Million People. *SSRN Electron. J.* (2021)
245 doi:10.2139/ssrn.3789264.
- 246 15. Case, J. B. *et al.* Neutralizing Antibody and Soluble ACE2 Inhibition of a Replication-Competent VSV-
247 SARS-CoV-2 and a Clinical Isolate of SARS-CoV-2. *Cell Host Microbe* **28**, 475–485.e5 (2020).
- 248 16. Liu, Y. *et al.* Neutralizing Activity of BNT162b2-Elicited Serum — Preliminary Report. *N. Engl. J. Med.*
249 NEJMc2102017 (2021) doi:10.1056/NEJMc2102017.

17. Chen, R. E. *et al.* Resistance of SARS-CoV-2 variants to neutralization by monoclonal and serum-derived polyclonal antibodies. *Nat. Med.* (2021) doi:10.1038/s41591-021-01294-w.
18. Leung, K., Shum, M. H., Leung, G. M., Lam, T. T. & Wu, J. T. Early transmissibility assessment of the N501Y mutant strains of SARS-CoV-2 in the United Kingdom, October to November 2020. *Eurosurveillance* **26**, (2021).
19. Turner, J. S. *et al.* Human germinal centres engage memory and naive B cells after influenza vaccination. *Nature* **586**, 127–132 (2020).
20. Pardi, N. *et al.* Expression kinetics of nucleoside-modified mRNA delivered in lipid nanoparticles to mice by various routes. *J. Controlled Release* **217**, 345–351 (2015).
21. Liang, F. *et al.* Efficient Targeting and Activation of Antigen-Presenting Cells In Vivo after Modified mRNA Vaccine Administration in Rhesus Macaques. *Mol. Ther.* **25**, 2635–2647 (2017).
22. Tai, W. *et al.* A novel receptor-binding domain (RBD)-based mRNA vaccine against SARS-CoV-2. *Cell Res.* **30**, 932–935 (2020).
23. Lederer, K. *et al.* SARS-CoV-2 mRNA Vaccines Foster Potent Antigen-Specific Germinal Center Responses Associated with Neutralizing Antibody Generation. *Immunity* **53**, 1281-1295.e5 (2020).
24. Hassan, A. O. *et al.* A Single-Dose Intranasal ChAd Vaccine Protects Upper and Lower Respiratory Tracts against SARS-CoV-2. *Cell* **183**, 169-184.e13 (2020).
25. Wrammert, J. *et al.* Rapid cloning of high-affinity human monoclonal antibodies against influenza virus. *Nature* **453**, 667–671 (2008).
26. Ellebedy, A. H. *et al.* Defining antigen-specific plasmablast and memory B cell subsets in human blood after viral infection or vaccination. *Nat. Immunol.* **17**, 1226–1234 (2016).
27. Krammer, F., Srivastava, K., the PARIS team & Simon, V. *Robust spike antibody responses and increased reactogenicity in seropositive individuals after a single dose of SARS-CoV-2 mRNA vaccine.*

273 <http://medrxiv.org/lookup/doi/10.1101/2021.01.29.21250653> (2021)

274 doi:10.1101/2021.01.29.21250653.

275 28. Gaebler, C. *et al.* Evolution of antibody immunity to SARS-CoV-2. *Nature* (2021) doi:10.1038/s41586-
276 021-03207-w.

277 29. Weisel, F. J., Zuccarino-Catania, G. V., Chikina, M. & Shlomchik, M. J. A Temporal Switch in the
278 Germinal Center Determines Differential Output of Memory B and Plasma Cells. *Immunity* **44**, 116–
279 130 (2016).

280 30. Qi, H., Cannons, J. L., Klauschen, F., Schwartzberg, P. L. & Germain, R. N. SAP-controlled T-B cell
281 interactions underlie germinal centre formation. *Nature* **455**, 764–9 (2008).

282 31. Plante, J. A. *et al.* Spike mutation D614G alters SARS-CoV-2 fitness. *Nature* (2020)
283 doi:10.1038/s41586-020-2895-3.

284 32. Xie, X. *et al.* An Infectious cDNA Clone of SARS-CoV-2. *Cell Host Microbe* **27**, 841-848.e3 (2020).

285 33. Stadlbauer, D. *et al.* SARS-CoV-2 Seroconversion in Humans: A Detailed Protocol for a Serological
286 Assay, Antigen Production, and Test Setup. *Curr. Protoc. Microbiol.* **57**, (2020).

287 34. Pallesen, J. *et al.* Immunogenicity and structures of a rationally designed prefusion MERS-CoV spike
288 antigen. *Proc. Natl. Acad. Sci.* **114**, E7348–E7357 (2017).

289 35. Liu, Z. *et al.* Identification of SARS-CoV-2 spike mutations that attenuate monoclonal and serum
290 antibody neutralization. *Cell Host Microbe* S1931312821000445 (2021)
291 doi:10.1016/j.chom.2021.01.014.

292 36. Wrammert, J. *et al.* Broadly cross-reactive antibodies dominate the human B cell response against
293 2009 pandemic H1N1 influenza virus infection. *J. Exp. Med.* **208**, 181–193 (2011).

294 37. Smith, K. *et al.* Rapid generation of fully human monoclonal antibodies specific to a vaccinating
295 antigen. *Nat. Protoc.* **4**, 372–384 (2009).

- 296 38. Nachbagauer, R. *et al.* Broadly Reactive Human Monoclonal Antibodies Elicited following Pandemic
297 H1N1 Influenza Virus Exposure Protect Mice against Highly Pathogenic H5N1 Challenge. *J. Virol.* **92**,
298 1–17 (2018).
- 299 39. Brochet, X., Lefranc, M.-P. & Giudicelli, V. IMGT/V-QUEST: the highly customized and integrated
300 system for IG and TR standardized V-J and V-D-J sequence analysis. *Nucleic Acids Res.* **36**, W503–
301 W508 (2008).
- 302 40. Giudicelli, V., Brochet, X. & Lefranc, M.-P. IMGT/V-QUEST: IMGT Standardized Analysis of the
303 Immunoglobulin (IG) and T Cell Receptor (TR) Nucleotide Sequences. *Cold Spring Harb. Protoc.* **2011**,
304 pdb.prot5633-pdb.prot5633 (2011).
- 305

Main Text Figure Legends

Figure 1. Plasmablast and antibody response to SARS-CoV-2 immunization.

a, Study design. Thirty-two healthy adult volunteers (ages 28–73, 7 with history of SARS-CoV-2 infection) were enrolled and received BNT162b2 mRNA SARS-CoV-2 vaccine. Blood was collected pre-immunization, and 3, 4, 5, and 7 weeks after immunization. For 12 participants (ages 28–52, none with history of SARS-CoV-2 infection), fine needle aspirates (FNAs) of ipsilateral axillary lymph nodes were collected 3, 4, 5, and 7 weeks after immunization. **b–c**, ELISpot quantification of S-binding IgG- (**b**) and IgA- (**c**) secreting plasmablasts (PBs) in blood at baseline, 3, 4, 5, and 7 weeks post-immunization in participants without (red) and with (black) history of SARS-CoV-2 infection. **d**, Plasma IgG titers against SARS-CoV-2 spike protein (S) (*left*) and the receptor binding domain (RBD) of S (*right*) measured by ELISA in participants without (red) and with (black) history of SARS-CoV-2 infection at baseline, 3, 4, 5, and 7 weeks post-immunization. **e**, Neutralizing activity of serum against WA1/2020 D614G (*left*), B.1.1.7 (*middle*), and a chimeric virus expressing B.1.351 spike (*right*) in Vero-TMPRSS2 cells at baseline, 3, and 5 or 7 weeks post-immunization in participants without (red) and with (black) history of SARS-CoV-2 infection. *P*-values from two-sided Mann-Whitney tests. Dotted lines indicate limits of detection. Horizontal lines indicate geometric mean. Symbols at each timepoint in **b–e** represent one sample (n=32). Results are from one experiment performed in duplicate.

Figure 2. Germinal center B cell response to SARS-CoV-2 immunization.

a, Representative Doppler ultrasound image of two draining LNs “1”, and “2” proximal to the axillary vein “LAX V” 5 weeks after immunization. **b and d**, Representative flow cytometry plots of Bcl6 and CD38 staining on IgD^{lo} CD19⁺ CD3[−] live singlet lymphocytes in FNA samples (**b**) and S staining on Bcl6⁺CD38^{int} GC B cells in tonsil and FNA samples (**d**) at the indicated times after immunization. **c and e**, Kinetics of total (**c**) and S⁺ (**e**) GC B cells as gated in **b** and **d**, respectively

from FNA of draining lymph nodes. Symbols at each timepoint represent one FNA sample (n = 12). **f**, Binding of mAbs generated from GC B cells to SARS-CoV-2 S, N-terminal domain of S, RBD, or spike proteins of betacoronavirus OC43 or HKU1 measured by ELISA. Bars indicate mean \pm SE. Baseline for area under the curve was set to the mean + three times the standard deviation of background binding to bovine serum albumin.

Figure 3. Lymph node plasmablast response to SARS-CoV-2 immunization.

a and c, Representative flow cytometry plots showing gating of CD20^{lo} CD38⁺ CD71⁺ Blimp1⁺ S⁺ PBs from IgD^{lo} CD19⁺ CD3⁻ live singlet lymphocytes (**a**) and IgA and IgM staining on S⁺ PBs (**d**) in FNA samples. **b**, Kinetics of S⁺ PBs as gated in **a** from FNA of draining lymph nodes. Symbols at each timepoint represent one FNA sample (n = 12). **d**, Percentages of IgM⁺ (teal), IgA⁺ (yellow), or IgM⁻IgA⁻ (purple) S⁺ PBs as gated in **c** from in FNA of draining lymph nodes 5 weeks after primary immunization. Each bar represents one FNA sample (n = 12).

Methods

Sample collection, preparation, and storage. All studies were approved by the Institutional Review Board of Washington University in St. Louis. Written consent was obtained from all participants. Thirty-two healthy volunteers were enrolled, of whom 12 provided axillary LN samples (**Extended Data Table 1**). Blood samples were collected in EDTA tubes, and peripheral blood mononuclear cells (PBMCs) were enriched by density gradient centrifugation over Ficoll 1077 (GE) or Lymphopure (BioLegend). The residual red blood cells were lysed with ammonium chloride lysis buffer, and cells were immediately used or cryopreserved in 10% dimethylsulfoxide in FBS. Ultrasound guided fine-needle aspiration (FNA) of axillary lymph nodes was performed by a radiologist or a qualified physician's assistant under the supervision of a radiologist. Lymph node dimensions and cortical thickness were measured, and the presence and degree of cortical vascularity and location of the lymph node relative to the axillary vein were determined prior to each FNA. For each FNA sample, six passes were made under continuous real-time ultrasound guidance using 25-gauge needles, each of which was flushed with 3 mL of RPMI 1640 supplemented with 10% FBS and 100 U/mL penicillin/streptomycin, followed by three 1-mL rinses. Red blood cells were lysed with ammonium chloride buffer (Lonza), washed with PBS supplemented with 2% FBS and 2 mM EDTA, and immediately used or cryopreserved in 10% dimethylsulfoxide in FBS. Participants reported no adverse effects from phlebotomies or serial FNAs.

Cell lines. Expi293F cells were cultured in Expi293 Expression Medium (Gibco). Vero-TMPRSS2 cells (a gift from Siyuan Ding, Washington University School of Medicine) were cultured at 37°C in Dulbecco's Modified Eagle medium (DMEM) supplemented with 10% fetal bovine serum (FBS), 10 mM HEPES pH 7.3, 1 mM sodium pyruvate, 1× non-essential amino acids, and 100 U/ml of penicillin–streptomycin.

Viruses. The 2019n-CoV/USA_WA1/2020 isolate of SARS-CoV-2 was obtained from the US Centers for Disease Control. The UK B.1.1.7 isolate was obtained from an infected individual.

The point mutation D614G in the spike gene was introduced into an infectious complementary DNA clone of the 2019n-CoV/USA_WA1/2020 strain as described previously³¹. Nucleotide substitutions were introduced into a subclone puc57-CoV-2-F5-7 containing the spike gene of the SARS-CoV-2 wild-type infectious clone³². The South African variant spike gene (B.1.351) was produced synthetically by Gibson assembly. The full-length infectious cDNA clones of the variant SARS-CoV-2 viruses were assembled by *in vitro* ligation of seven contiguous cDNA fragments following the previously described protocol³². *In vitro* transcription was then performed to synthesize full-length genomic RNA. To recover the mutant viruses, the RNA transcripts were electroporated into Vero E6 cells. The viruses from the supernatant of cells were collected 40-h later and served as p0 stocks. All viruses were passaged once in Vero-hACE2-TMPRSS2 cells and subjected to deep sequencing after RNA extraction to confirm the introduction and stability of substitutions¹⁸. All virus preparation and experiments were performed in an approved Biosafety level 3 (BSL-3) facility.

Antigens. Recombinant soluble SARS-CoV-2 spike (S) protein, recombinant receptor binding domain of S (RBD), human coronavirus OC43 spike, and human coronavirus HKU1 spike were expressed as previously described³³. Briefly, mammalian cell codon-optimized nucleotide sequences coding for the soluble ectodomain of the spike protein of SARS-CoV-2 (GenBank: MN908947.3, amino acids 1-1213) including a C-terminal thrombin cleavage site, T4 foldon trimerization domain, and hexahistidine tag and for the receptor binding domain (RBD, amino acids 319-541) along with the signal peptide (amino acids 1-14) plus a hexahistidine tag were cloned into mammalian expression vector pCAGGS. The spike protein sequence was modified to remove the polybasic cleavage site (RRAR to A), and two pre-fusion stabilizing proline mutations were introduced (K986P and V987P, wild type numbering). Expression plasmids encoding for the spike of common human coronaviruses OC43 and HKU1 were provided by Barney Graham (NIH, Bethesda, MD)³⁴. Recombinant proteins were produced in Expi293F cells (ThermoFisher) by transfection with purified DNA using the ExpiFectamine 293 Transfection Kit (ThermoFisher).

Supernatants from transfected cells were harvested 3 days post-transfection, and recombinant proteins were purified using Ni-NTA agarose (ThermoFisher), then buffer exchanged into phosphate buffered saline (PBS) and concentrated using Amicon Ultracel centrifugal filters (EMD Millipore). For flow cytometry staining, recombinant S was labeled with Alexa Fluor 647-NHS ester or biotinylated using the EZ-Link Micro NHS-PEG4-Biotinylation Kit (Thermo Fisher); excess Alexa Fluor 647 and biotin were removed using 7-kDa Zeba desalting columns (Pierce).

ELISpot. Plates were coated with Flucelvax Quadrivalent 2019/2020 seasonal influenza virus vaccine (Seqirus), S, or RBD. A direct *ex-vivo* ELISpot was performed to determine the number of total, vaccine-binding, or recombinant S-binding IgG- and IgA-secreting cells present in PBMC samples using IgG/IgA double-color ELISpot Kits (Cellular Technologies, Ltd.) according to the manufacturer's instructions. ELISpot plates were analyzed using an ELISpot counter (Cellular Technologies Ltd.).

ELISA. Assays were performed in 96-well plates (MaxiSorp; Thermo) coated with 100 μ L of recombinant S, RBD, N-terminal domain of S (SinoBiological), OC43 spike, HKU1 spike, or bovine serum albumin diluted to 1 μ g/mL in PBS, and plates were incubated at 4°C overnight. Plates then were blocked with 10% FBS and 0.05% Tween 20 in PBS. Plasma or purified mAbs were serially diluted in blocking buffer and added to the plates. Plates were incubated for 90 min at room temperature and then washed 3 times with 0.05% Tween 20 in PBS. Goat anti-human IgG-HRP (Jackson ImmunoResearch, 1:2,500) was diluted in blocking buffer before adding to wells and incubating for 60 min at room temperature. Plates were washed 3 times with 0.05% Tween 20 in PBS and 3 times with PBS before the addition of peroxidase substrate (SigmaFAST o-phenylenediamine dihydrochloride, Sigma-Aldrich). Reactions were stopped by the addition of 1 M hydrochloric acid. Optical density measurements were taken at 490 nm. The area under the curve for each mAb and half-maximal binding dilution for each plasma sample were calculated using Graphpad Prism v8.

Focus reduction neutralization test. Plasma samples were declotted by diluting 1:10 in DMEM supplemented with 2% FBS, 10 mM HEPES, and 100 U/mL penicillin/streptomycin and incubating for 3 h at 37°C. Serial dilutions of resulting serum were incubated with 10² focus-forming units (FFU) of different strains or variants of SARS-CoV-2 for 1 h at 37°C. Antibody-virus complexes were added to Vero-TMPRSS2 cell monolayers in 96-well plates and incubated at 37°C for 1 h. Subsequently, cells were overlaid with 1% (w/v) methylcellulose in MEM supplemented with 2% FBS. Plates were harvested 24 h later by removing overlays and fixed with 4% PFA in PBS for 20 min at room temperature. Plates were washed and sequentially incubated with an oligoclonal pool of SARS2-2, SARS2-11, SARS2-16, SARS2-31, SARS2-38, SARS2-57, and SARS2-71 anti-S antibodies³⁵ and HRP-conjugated goat anti-mouse IgG in PBS supplemented with 0.1% saponin and 0.1% bovine serum albumin. SARS-CoV-2-infected cell foci were visualized using TrueBlue peroxidase substrate (KPL) and quantitated on an ImmunoSpot microanalyzer (Cellular Technologies).

Cell sorting and flow cytometry. Staining for flow cytometry analysis and sorting was performed using freshly isolated or cryo-preserved FNA or tonsil samples. For analysis, cells were incubated for 30 min on ice with biotinylated and Alexa Fluor 647 conjugated recombinant soluble S and PD-1-BB515 (EH12.1, BD Horizon, 1:100) in 2% FBS and 2 mM EDTA in PBS (P2), washed twice, then stained for 30 min on ice with IgG-BV480 (goat polyclonal, Jackson ImmunoResearch, 1:100), IgA-FITC (M24A, Millipore, 1:500), CD45-A532 (HI30, Thermo, 1:50), CD38-BB700 (HIT2, BD Horizon, 1:500), CD20-Pacific Blue (2H7, 1:400), CD8-BV570 (RPA-T8, 1:200), IgM-BV605 (MHM-88, 1:100), HLA-DR-BV650 (L243, 1:100), CD19-BV750 (HIB19, 1:100), CXCR5-PE-Dazzle 594 (J252D4, 1:50), IgD-PE-Cy5 (IA6-2, 1:200), CD14-PerCP (HCD14, 1:50), CD71-PE-Cy7 (CY1G4, 1:400), CD4-Spark685 (SK3, 1:200), streptavidin-APC-Fire750, CD3-APC-Fire810 (SK7, 1:50), and Zombie NIR (all BioLegend) diluted in Brilliant Staining buffer (BD Horizon). Cells were washed twice with P2, fixed for 1 h at 25°C using the True Nuclear fixation kit (BioLegend), washed twice with True Nuclear Permeabilization/Wash buffer, stained with FoxP3-BV421 (206D,

BioLegend, 1:15), Ki-67-BV711 (Ki-67, BioLegend, 1:200), Tbet-BV785 (4B10, BioLegend, 1:400), Bcl6-PE (K112-91, BD Pharmingen, 1:25), and Blimp1-A700 (646702, R&D, 1:50) for 1h at 25°C, washed twice with True Nuclear Permeabilization/Wash buffer, and acquired on an Aurora using SpectroFlo v2.2 (Cytex). Flow cytometry data were analyzed using FlowJo v10 (Treestar).

For sorting, cells were stained for 30 min on ice with CD19-BV421 (HIB19, 1:100), CD3-FITC (HIT3a, 1:200), IgD-PerCP-Cy5.5 (IA6-2, 1:200), CD71-PE (CY1G4, 1:400), CXCR5-PE-Dazzle 594 (J252D4, 1:50), CD38-PE-Cy7 (HIT2, 1:200), CD20-APC-Fire750 (2H7, 1:100), Zombie Aqua (all BioLegend), and Alexa Fluor 647 conjugated recombinant soluble S. Cells were washed twice, and single S-binding GC B cells (live singlet CD3⁻ CD19⁺ IgD^{lo} CD38^{int} CD20^{hi} CD71⁺ CXCR5⁺ S⁺) were sorted using a FACS Aria II into 96-well plates containing 2 μ L Lysis Buffer (Clontech) supplemented with 1 U/ μ L RNase inhibitor (NEB) and immediately frozen on dry ice.

Monoclonal antibody (mAb) generation. Antibodies were cloned as described previously³⁶. Briefly, VH, V κ , and V λ genes were amplified by reverse transcription-PCR and nested PCR reactions from singly-sorted GC B cells using primer combinations specific for IgG, IgM/A, Ig κ , and Ig λ from previously described primer sets³⁷ and then sequenced. To generate recombinant antibodies, restriction sites were incorporated via PCR with primers to the corresponding heavy and light chain V and J genes. The amplified VH, V κ , and V λ genes were cloned into IgG1 and Ig κ or Ig λ expression vectors, respectively, as described previously^{25,37,38}. Heavy and light chain plasmids were co-transfected into Expi293F cells (Gibco) for expression, and antibody was purified using protein A agarose chromatography (Goldbio). Sequences were obtained from PCR reaction products and annotated using the ImMunoGeneTics (IMGT)/V-QUEST database (http://www.imgt.org/IMGT_vquest/)^{39,40}. Sequences were determined to be clonally related if they shared Vh and Jh genes, had identical complementarity determining region

472 (CDR) lengths, and no more than 3 amino acid differences in the CDR3. Mutation frequency was
473 calculated by counting the number of nonsynonymous nucleotide mismatches from the germline
474 sequence in the heavy chain variable segment leading up to the CDR3, while excluding the 5'
475 primer sequences that could be error-prone.

ACKNOWLEDGEMENTS

We thank the generous participation of the donors for providing specimens. We thank Lisa Kessels, AJ Winingham, Khatira Safi, and the staff of the Infectious Diseases Clinical Research Unit at Washington University School of Medicine for assistance with scheduling participants and sample collection. The Vero-TMPRSS2 cells were kindly provided by Siyuan Ding (Washington University School of Medicine, St. Louis, MO). The expression plasmids encoding for the spike of coronaviruses OC43 and HKU1 were kindly provided by Kizzmekia Corbett and Barney Graham (NIH, Bethesda, MD). We thank Julian Q. Zhou for critical reading of the manuscript.

The Ellebedy laboratory was supported by NIAID grant U01AI141990, U01AI150747, NIAID Centers of Excellence for Influenza Research and Surveillance contract HHSN272201400006C. The Ellebedy and Krammer laboratories were supported by NIAID Centers of Excellence for Influenza Research and Surveillance contract HHSN272201400008C, and NIAID Collaborative Influenza Vaccine Innovation Centers contract 75N93019C00051. The Diamond laboratory was supported by R01 AI157155. The Shi laboratory was supported by NIH grants AI134907 and UL1TR001439, and awards from the Sealy & Smith Foundation, Kleberg Foundation, the John S. Dunn Foundation, the Amon G. Carter Foundation, the Gilson Longenbaugh Foundation, and the Summerfield Robert Foundation. J.S.T. was supported by NIAID 5T32CA009547. J.B.C. was supported by a Helen Hay Whitney Foundation postdoctoral fellowship.

The WU368 study was reviewed and approved by the Washington University Institutional Review Board (approval no. 202012081).

AUTHOR CONTRIBUTIONS

A.H.E., J.A.O and R.M.P. conceived and designed the study. J.A.O., A.H., M.K.K., and R.M.P. wrote and maintained the IRB protocol, recruited, and phlebotomized participants and coordinated sample collection. J.S.T., E.K., W.K., A.J.S., T.L., M.T., R.E.C., and J.B.C. performed

experiments. T.S. and W.D.M performed FNA. W.D.M. and S.A.T. supervised lymph node evaluation prior to FNA and specimen collection and evaluated lymph node ultrasound data. F.A. and F.K. expressed CoV S proteins. J.S.T. sorted cells and collected and analysed the flow cytometry data. A.J.S. expressed the S and RBD proteins. X.X. and P.-Y.S. prepared the SARS-CoV-2 with variant spike mutations. J.S.T., A.M.R., and A.H.E. analyzed the data. M.S.D. and A.H.E. supervised experiments and obtained funding. J.S.T. and A.H.E. composed the manuscript. All authors reviewed the manuscript.

COMPETING INTERESTS

The Ellebedy laboratory received funding under sponsored research agreements that are unrelated to the data presented in the current study from Emergent BioSolutions and from AbbVie. A.H.E. is a consultant for Mubadala Investment Company. M.S.D. is a consultant for Inbios, Vir Biotechnology, NGM Biopharmaceuticals, and Carnival Corporation, and on the Scientific Advisory Boards of Moderna and Immunome. The Diamond laboratory has received unrelated funding support in sponsored research agreements from Moderna, Vir Biotechnology, and Emergent BioSolutions. A patent application related to this work has been filed by Washington University School of Medicine. The Icahn School of Medicine at Mount Sinai has filed patent applications relating to SARS-CoV-2 serological assays and NDV-based SARS-CoV-2 vaccines which list Florian Krammer as co-inventor. Mount Sinai has spun out a company, Kantaro, to market serological tests for SARS-CoV-2. Florian Krammer has consulted for Merck and Pfizer (before 2020), and is currently consulting for Pfizer, Seqirus and Avimex. The Krammer laboratory is also collaborating with Pfizer on animal models of SARS-CoV-2. The Shi laboratory has received sponsored research agreements from Pfizer, Gilead, Merck and IGM Sciences Inc. The content of this manuscript is solely the responsibility of the authors and does not necessarily represent the official view of NIAID or NIH.

528 **Data availability statement**

529 Antibody sequences are deposited on GenBank under the following accession numbers: [xx],
530 available from GenBank/EMBL/DDBJ. Other relevant data are available from the corresponding
531 author upon request.

532 **Extended Data Figure Legends**

533 **Extended Data Figure 1. Gating strategy for S-binding germinal center B cells**

534 **a**, Sorting gating strategy for S-binding GC B cells in FNA samples. **b**, Representative plot of GC
535 B cells in tonsil.

536

537 **Extended Data Table Titles and Footnotes**

538

539 **Extended Data Table 1. Participant demographics**

540 **Extended Data Table 2. Vaccine side effects**

541 **Extended Data Table 3. Immunoglobulin gene usage of S-binding mAbs**

542 *Denominator is number of Vh sequences extending into CDR3 per participant

543 **V-region nonsynonymous nucleotide substitutions

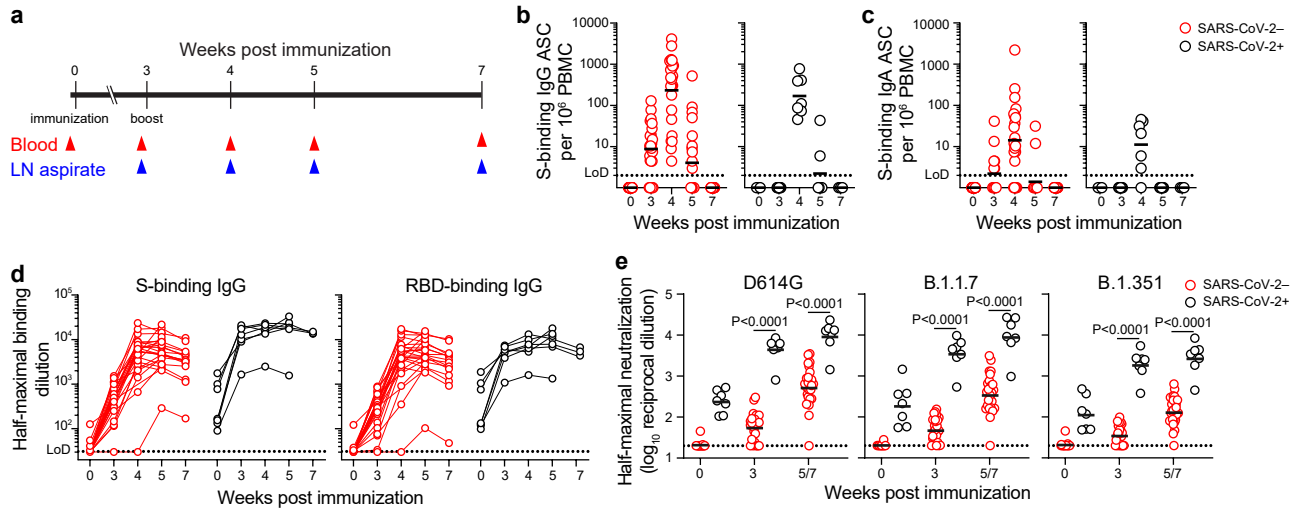


Figure 1. Plasmablast and antibody response to SARS-CoV-2 immunization.

a, Study design. Thirty-two healthy adult volunteers (ages 28–73, 7 with history of SARS-CoV-2 infection) were enrolled and received BNT162b2 mRNA SARS-CoV-2 vaccine. Blood was collected pre-immunization, and 3, 4, 5, and 7 weeks after immunization. For 12 participants (ages 28–52, none with history of SARS-CoV-2 infection), fine needle aspirates (FNAs) of ipsilateral axillary lymph nodes were collected 3, 4, 5, and 7 weeks after immunization. **b–c**, ELISpot quantification of S-binding IgG- (**b**) and IgA- (**c**) secreting plasmablasts (PBs) in blood at baseline, 3, 4, 5, and 7 weeks post-immunization in participants without (red) and with (black) history of SARS-CoV-2 infection. **d**, Plasma IgG titers against SARS-CoV-2 spike protein (S) (*left*) and the receptor binding domain (RBD) of S (*right*) measured by ELISA in participants without (red) and with (black) history of SARS-CoV-2 infection at baseline, 3, 4, 5, and 7 weeks post-immunization. **e**, Neutralizing activity of serum against WA1/2020 D614G (*left*), B.1.1.7 (*middle*), and a chimeric virus expressing B.1.351 spike (*right*) in Vero-TMPRSS2 cells at baseline, 3, and 5 or 7 weeks post-immunization in participants without (red) and with (black) history of SARS-CoV-2 infection. P -values from two-sided Mann-Whitney tests. Dotted lines indicate limits of detection. Horizontal lines indicate geometric mean. Symbols at each timepoint in **b–e** represent one sample ($n=32$). Results are from one experiment performed in duplicate.

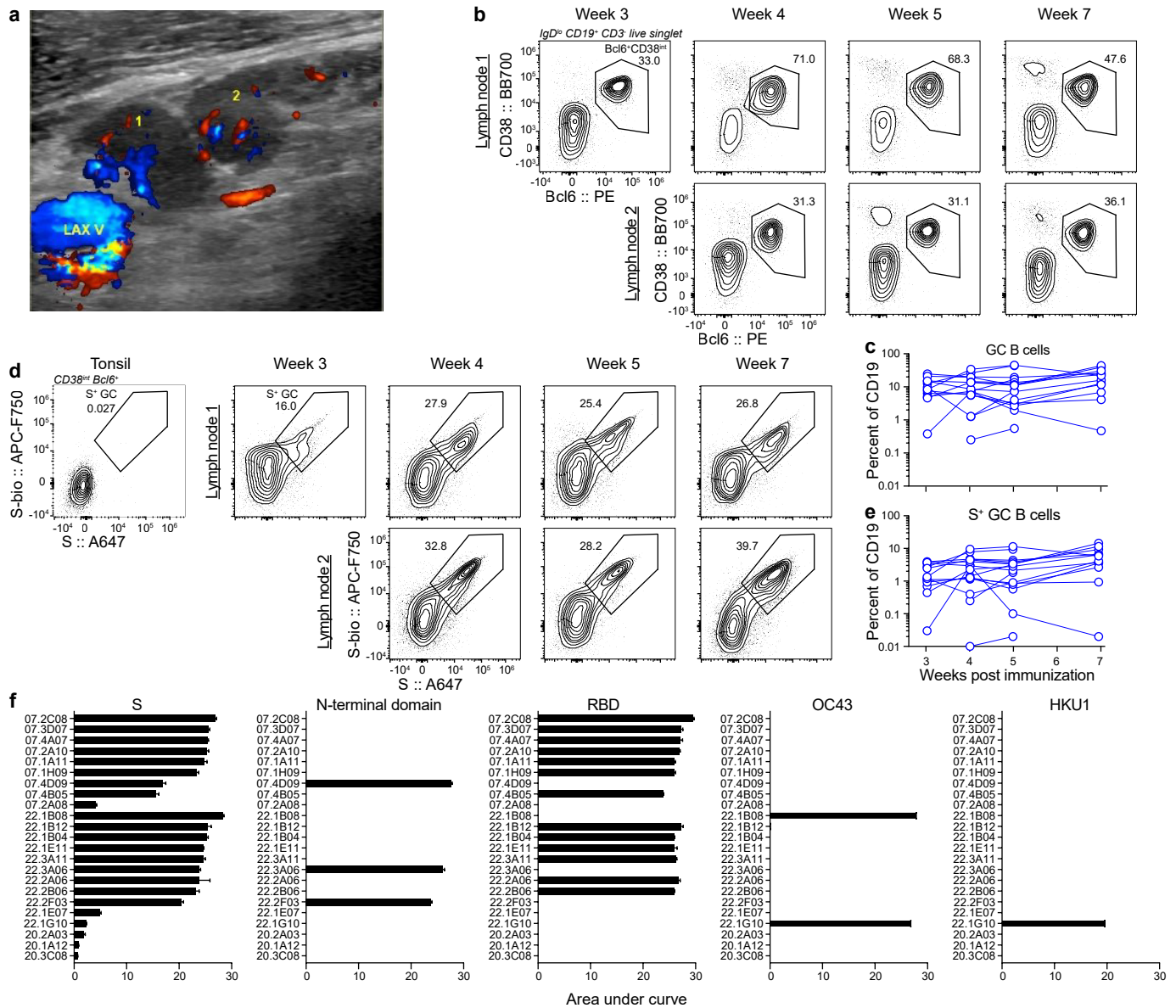


Figure 2. Germinal center B cell response to SARS-CoV-2 immunization.

a, Representative Doppler ultrasound image of two draining LNs "1", and "2" proximal to the axillary vein "LAX V" 5 weeks after immunization. **b** and **d**, Representative flow cytometry plots of Bcl6 and CD38 staining on IgD^{lo} CD19⁺ CD3⁻ live singlet lymphocytes in FNA samples (**b**) and S staining on Bcl6⁺CD38^{int} GC B cells in tonsil and FNA samples (**d**) at the indicated times after immunization. **c** and **e**, Kinetics of total (**c**) and S⁺ (**e**) GC B cells as gated in **b** and **d**, respectively from FNA of draining lymph nodes. Symbols at each timepoint represent one FNA sample (n = 12). **f**, Binding of mAbs generated from GC B cells to SARS-CoV-2 S, N-terminal domain of S, RBD, or spike proteins of betacoronavirus OC43 or HKU1 measured by ELISA. Bars indicate mean \pm SE. Baseline for area under the curve was set to the mean + three times the standard deviation of background binding to bovine serum albumin.

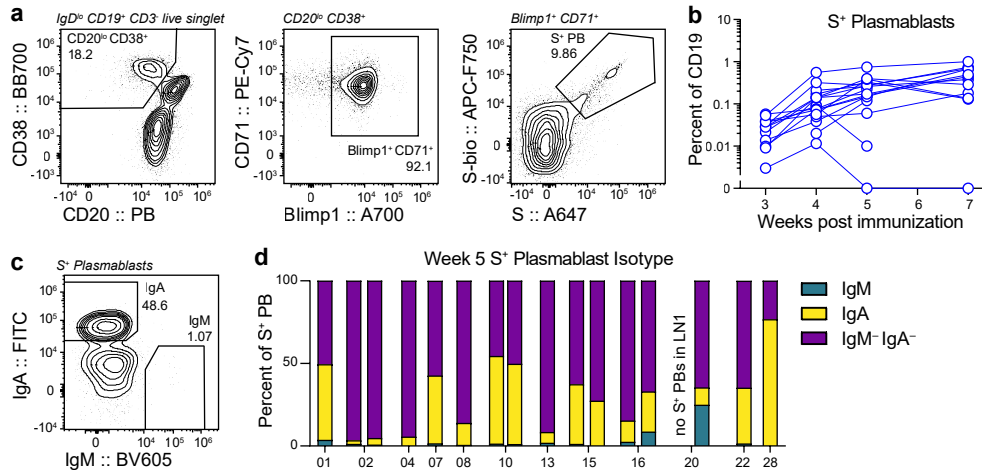
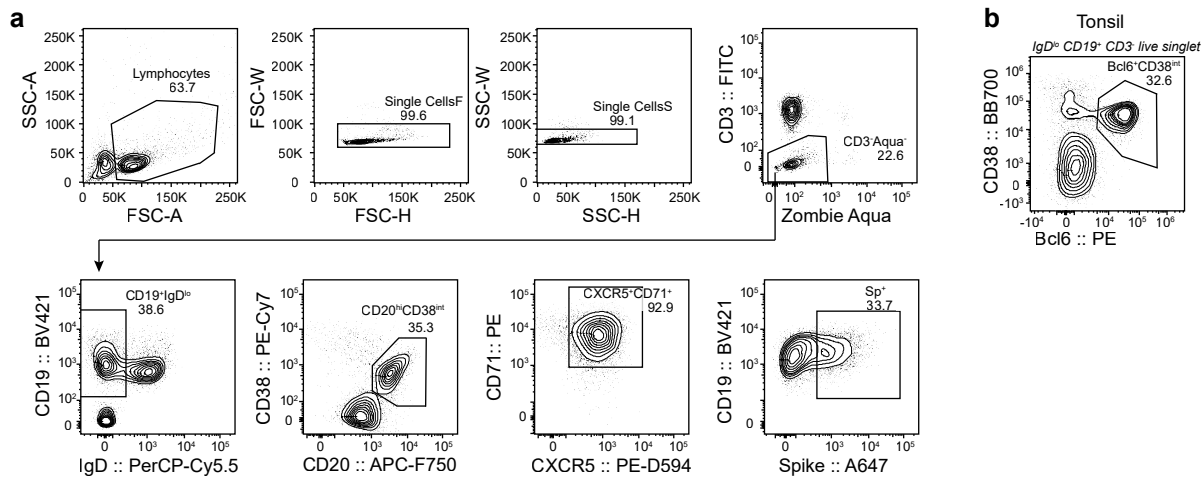


Figure 3. Lymph node plasmablast response to SARS-CoV-2 immunization.

a and c, Representative flow cytometry plots showing gating of CD20^{lo} CD38⁺ CD71⁺ Blimp1⁺ S⁺ PBs from IgD^{lo} CD19⁺ CD3⁻ live singlet lymphocytes (**a**) and IgA and IgM staining on S⁺ PBs (**c**) in FNA samples. **b**, Kinetics of S⁺ PBs as gated in **a** from FNA of draining lymph nodes. Symbols at each timepoint represent one FNA sample (n = 12). **d**, Percentages of IgM⁺ (teal), IgA⁺ (yellow), or IgM⁻IgA⁻ (purple) S⁺ PBs as gated in **c** from in FNA of draining lymph nodes 5 weeks after primary immunization. Each bar represents one FNA sample (n = 12).



Extended Data Figure 1. Gating strategy for S-binding germinal center B cells

a, Sorting gating strategy for S-binding GC B cells in FNA samples. **b**, Representative plot of GC B cells in tonsil.

544 **Extended Data Table 1. Participant demographics**

Variable	Total N=32 N (%)	Lymph node N=12 N (%)
Age (median [range])	37 (28-73)	36.5 (28-52)
Sex		
Female	16 (50)	7 (58.3)
Male	16 (50)	5 (41.7)
Race		
White	25 (78.1)	10 (83.3)
Asian	5 (15.6)	1 (8.3)
Black	1 (3.1)	1 (8.3)
Other	1 (3.1)	0 (0)
Ethnicity		
Not of Hispanic, Latinx, or Spanish origin	30 (93.8)	11 (91.7)
Hispanic, Latinx, Spanish origin	2 (6.3)	1 (8.3)
BMI (median [range])	25.3 (21.4-40)	23.5 (21.4-40)
Comorbidities		
Lung disease	2 (6.3)	1 (8.3)
Diabetes mellitus	0 (0)	0 (0)
Hypertension	5 (15.6)	2 (16.7)
Cardiovascular	0 (0)	0 (0)
Liver disease	0 (0)	0 (0)
Chronic kidney disease	0 (0)	0 (0)
Cancer on chemotherapy	0 (0)	0 (0)
Hematological malignancy	0 (0)	0 (0)
Pregnancy	0 (0)	0 (0)
Neurological	0 (0)	0 (0)
HIV	0 (0)	0 (0)
Solid organ transplant recipient	0 (0)	0 (0)
Bone marrow transplant recipient	0 (0)	0 (0)
Hyperlipidemia	1 (3.1)	0 (0)
Confirmed SARS-CoV-2 infection	7 (21.9)	0 (0)
Time from SARS-CoV-2 infection to baseline visit in days (median [range])	106 (50-230)	--

545 **Extended Data Table 2. Vaccine side-effects**

546

Variable	Total N=32 N (%)		Total N=32 N (%)
First dose		Second dose	
None	4 (12.5)	None	2 (6.2)
Chills	5 (15.6)	Chills	10 (31.3)
Fever	2 (6.3)	Fever	5 (15.6)
Headache	5 (15.6)	Headache	9 (28.1)
Injection site pain	25 (78.1)	Injection site pain	27 (84.4)
Muscle or joint pain	7 (21.9)	Muscle or joint pain	16 (50)
Fatigue	7 (21.9)	Fatigue	14 (43.8)
Sweating	0 (0)	Sweating	2 (6.3)
Duration of side effects in hours (median [range])			
Chills	48 (6-72)	Chills	21 (4-48)
Fever	9 (6-12)	Fever	24 (1-48)
Headache	12 (5-48)	Headache	24 (4-48)
Injection site pain	36 (2-120)	Injection site pain	36 (2-96)
Muscle or joint pain	36 (0-48)	Muscle or joint pain	31.5 (1-48)
Fatigue	36 (5-48)	Fatigue	25.5 (2-144)
Sweating	0 (0)	Sweating	18 (18)

Extended Data Table 3. Immunoglobulin gene usage of S-binding mAbs

Name	Clone Size*	Native Isotype	Heavy chain			Light chain		
			Gene usage	Mutations**	HCDR3 AA sequence	Gene usage	Mutations**	LCDR3 AA sequence
07.1A11	1/21	IgM	VH3-15 DH1-7 JH4	4/283=0.0141	CTTGWFTGTYGDYFDYW	VK1-33 JK4	1/267=0.0037	CQQYDNLPPTF
07.1H09	1/21	IgG1	VH3-66 DH3-10 JH3	3/275=0.0109	CARDFREGAFDIW	VK1-9 JK4	0/266=0	CQQLNSYPPTF
07.2A08	1/21	IgG1	VH4-4 DH6-19 JH4	2/275=0.0073	CATDGGWYTFDHW	VL3-1 JL2	3/265=0.0113	CQAWGSSTVVF
07.2A10	1/21	IgG1	VH4-31 DH3-16 JH3	1/278=0.0036	CARYPVWGAFDIW	VK1-33 JK3	3/267=0.0112	CQHYDNLPPTF
07.2C08	1/21	IgG1	VH1-58 DH2-15 JH3	2/275=0.0073	CAAAAYCSGGSCSDGFDIW	VK3-20 JK1	5/266=0.0188	CQQYGSSPWTF
07.3D07	2/21	IgG1	VH3-30 DH5-18 JH4	3/277=0.0108	CARVLWLRGMFDYW	VL6-57 JL3	2/278=0.0072	CQSYDISNHVVF
07.4A07	1/21	IgG1	VH3-30 DH3-10 JH4	3/277=0.0108	CARGDY YSGSYPGKTFDYW	VK1-33 JK4	1/266=0.0038	CQQYDNLPLTF
07.4B05	1/21	IgG1	VH1-69 DH1-26 JH5	1/277=0.0036	CARGRLDSYSGSYYSWFDPW	VK4-1 JK2	2/283=0.0071	CQQYYSTPYTF
07.4D09	1/21	IgG1	VH4-4 DH2-15 JH4	1/274=0.0036	CATKYCSGGSCSYFGYW	VL2-23 JL3	0/277=0	CCSYAGSSTWVF
20.1A12	23/46	IgG1	VH3-30 DH1-26 JH4	2/277=0.0072	CAKGHSGSYRAPFDYW	VK3-20 JK2	0/263=0	CQQYGSSYTF
20.2A03	5/46	IgM	VH3-33 DH3-10 JH4	1/278=0.0036	CAREAYFGSGSSPDYW	VL3-10 JL2	2/272=0.0074	CYSTDSSDNHRRVF
20.3C08	2/46	IgG1	VH3-7 DH3-22 JH4	1/278=0.0036	CAREGTYYYDSSAYYNGGLDYW	VL3-10 JL1	1/272=0.0037	CYSTDSSGNHRRLF
22.1A12	3/55	IgG1	VH3-30 DH2-15 JH4	4/274=0.0146	CAKQGGGTYCGGGSCYRGYFDYW	VK1-33 JK4	2/264=0.0076	CQQYDNIPLTF
22.1B08	1/55	IgA1	VH1-46 DH4-17 JH3	16/278=0.0576	CARDPRVPAVTNVNDAFDLW	VK3-11 JK2	5/267=0.0187	CQQRSNRPPRWTF
22.1B12	1/55	IgG1	VH3-53 DH3-10 JH4	8/273=0.0293	CARSHLEVVRGVFDNW	VK4-1 JK2	1/282=0.0035	CQQYYSTPCSF
22.1E07	1/55	IgA1	VH3-33 DH4-17 JH4	3/278=0.0108	CAREGVYGDIGGAGLDYW	VL3-10 JL1	4/272=0.0147	CYSTDSSVNGRVF
22.1E11	1/55	IgG1	VH3-30 DH2-15 JH4	2/274=0.0073	CAKMGGVYCSAGNCYSGRLEYW	VK1-33 JK3	0/263=0	CQQYDNLLET
22.1G10	2/55	IgG1	VH4-59 DH2-21 JH5	12/275=0.0436	CARETVNNWVDPW	VK4-1 JK1	10/282=0.0355	CQQYFTTPWTF
22.2A06	6/55	IgG3	VH5-51 DH3-3 JH4	1/277=0.0036	CARREWGGSLGHIDYW	VL6-57 JL2	4/276=0.0145	CQSFSSNVVF
22.2B06	2/55	IgM	VH3-53 DH1-1 JH6	2/275=0.0073	CARDLQLYGMDVW	VL3-21 JL2	2/268=0.0075	CQVWDSSDPVVF
22.2F03	1/55	IgM	VH1-18 DH6-13 JH6	1/277=0.0036	CARVPGLVGYSSSWYDNEKNYYYYYYGMDVW	VL3-25 JL1	1/270=0.0037	CQSADSSGTYYVF
22.3A06	1/55	IgG1	VH3-23 DH5-18 JH5	2/277=0.0072	CAKADTAMAWYNWFDPW	VK3-11 JK4	3/264=0.0114	CQHRSNWPLTF
22.3A11	1/55	IgG1	VH4-34 DH7-27 JH2	1/270=0.0037	CARVWVRWWYFDLW	VL3-21 JL1	4/272=0.0147	CQVWDNSSDQPNYVF

*Denominator is number of Vh sequences extending into CDR3 per participant

**V-region nonsynonymous nucleotide substitutions